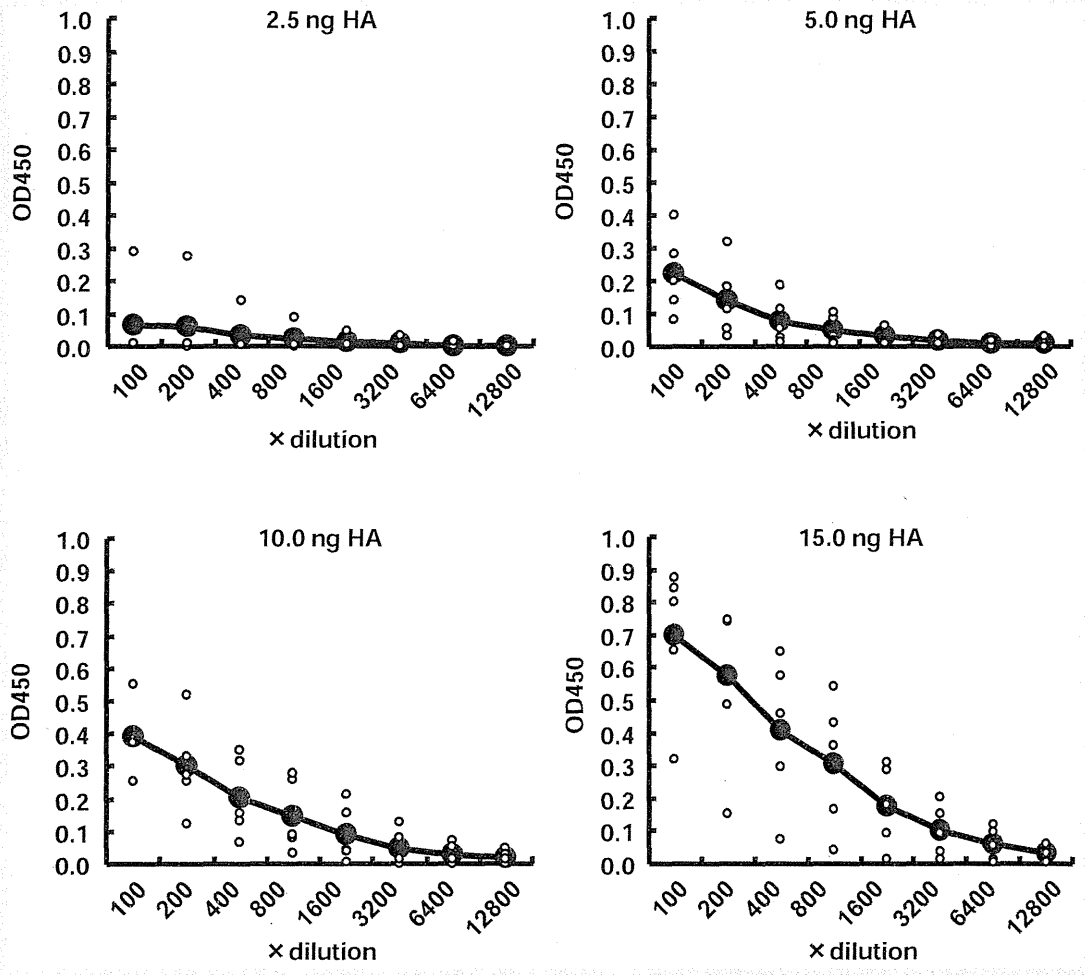

Figure 1: The amount of HA-specific IgG production by vaccination. Mice were fed an AIN-93M diet and given subcutaneous vaccination at doses between 2.5 and 15.0 ng HA and boosted on day 28 from the initial vaccination. Two weeks after the last vaccination, plasma was collected from each mouse, and the amount of HA-specific IgG antibody was measured by ELISA, as described in Materials and Methods. Values are means of 5 mice in each group. Open circles are individual data, closed circles are mean values.

production from peritoneal macrophages in vitro and enhances the activity of NK cells *in vivo* [12]. Koizumi et al. also reported that S-PT84 stimulates IFN-γ and IL-12 production through Toll-like receptor (TLR)-2 and TLR-4 on dendritic cells [16]. Moreover, Izumo et al. reported that *Salmonella*-specific antibody is enhanced by S-PT84 ingestion in *Salmonella* typhimurium-infected mice [17]. Accordingly, we thought that antigen-presenting cells were activated by ingestion of S-PT84 in this experiment, and production of HA-specific IgG in plasma may be enhanced, as in a previous report [17]. It is well known that influenza vaccines administered intramuscularly or subcutaneously induce a predominantly IgG-mediated protection in the systemic immune compartment, but this systemic immunization offers inadequate induction of IgA in airway mucosa [18]. Therefore, oral administration of S-PT84 might affect HA antigen-induced dendritic cell-mediated systemic immunity and induce HA-specific IgG in plasma, but not affect mucosal immunity and HA-specific IgA production.

The present data suggest that S-PT84 enhances antibody production as an adjuvant with limited dose of influenza viral antigen. Hui-Tsu et al. reported that the induction of HA-specific antibody in plasma was enhanced by IAV HA (H1N1) vaccination at 10 ng dose in mice, and the survival rate was also significantly improved by this vaccination [19]. The optimal density (OD) level of HA-specific IgG was similar compared with our present study. Moreover, the strain of IAV/California/7/2009 (H1N1) was same in both experiments. Therefore, we speculate that HA-specific antibody production level by the killed bacterial adjuvant S-PT84 might be sufficient for the viral protection and then an ample titer was obtained for influenza virus exclusion. It suggests that S-PT84 may decrease the risk of influenza virus re-infection treated with anti-viral neuraminidase inhibitors.

As a next step, it should be to investigate whether oral administration of S-PT84 together with the vaccination on limited dose of HA antigen can protect IAV infection, and/or whether oral administration of S-PT84 can induce sufficiently HA-specific IgG antibody treated with antiviral neuraminidase inhibitors after IAV infection.

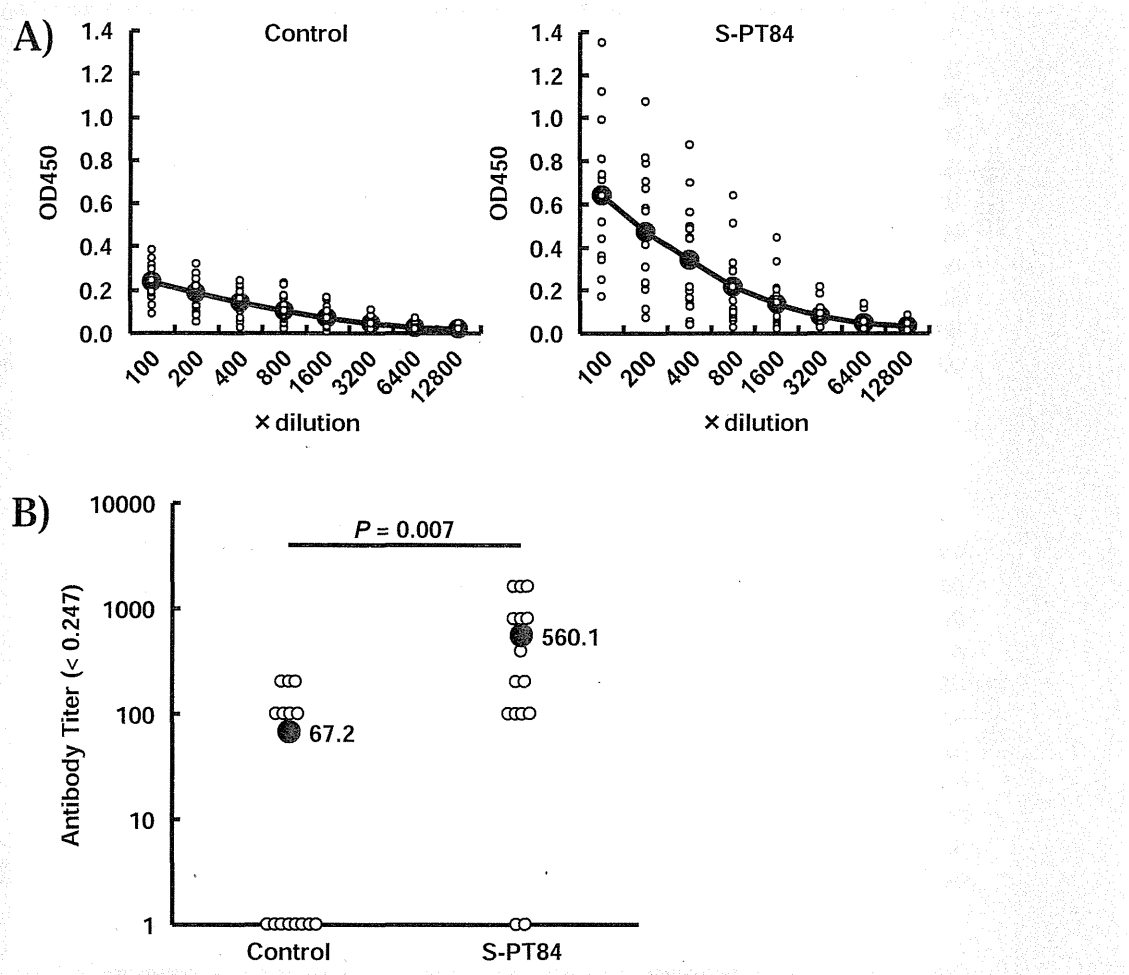

Figure 2: Effect of *Lactobacillus pentosus* strain S-PT84 on HA-specific IgG production by vaccination. Mice were fed an AIN-93M diet with or without 0.186% S-PT84 for 6 weeks followed by subcutaneous vaccination of 2.5 ng HA and boosted on day 28 from the initial vaccination. Two weeks after the last vaccination, plasma was collected from each mouse, and the amount of HA-specific IgG Antibody (Ab) **(A)** was measured by ELISA and expressed as the titer **(B)**, as described in Materials and Methods. Values are means of 15 mice in each group. Significant differences are seen between the control group and the S-PT84 group. Open circles are individual data, closed circles are mean values.

Japan is becoming a super-aging society more rapidly than other countries. Elderly persons have a high risk of influenza-associated pneumonia, which is sometimes fatal. Thus, management of influenza outbreaks is important for them. Indeed, seroconversion and seroprotection are lower in elderly individuals than in adults after influenza vaccination, and their immune functions are weaker than in adults [20]. It is important that preventive action be taken to enhance immune function or provide vaccination for the elderly. In this regard, S-PT84 may have a potential to improve their immune response.

References

1. Gillim-Ross L, Subbarao K (2006) Emerging respiratory viruses: challenges and vaccine strategies. Clin Microbiol Rev 19: 614-636.
2. Moscona A (2005) Neuraminidase inhibitors for Influenza. N Engl J Med 353: 1363-1373.
3. Shinahara W, Takahashi E, Sawabuchi T, Arai M, Hirotsu N, et al. (2013) Immunomodulator clarithromycin enhances mucosal and systemic immune responses and reduces re-infection rate in pediatric patients with Influenza treated with antiviral neuraminidase inhibitors: A retrospective analysis. PLoS One 8: e70060.
4. Blum S, Haller D, Pfeifer A, Schiffrin EJ (2002) Probiotics and immune response. Clin Rev Allergy Immunol 22: 287-309.
5. Perdigón G, Fuller R, Raya R (2001) Lactic acid bacteria and their effect on the immune system. Curr Issues Intest Microbiol 2: 27-42.
6. Yasui H, Kiyoshima J, Hori T (2004) Reduction of influenza virus titer and protection against influenza virus infection in infant mice fed *Lactobacillus casei* Shirota. Clin Diagn Lab Immunol 11: 675-679.
7. Maeda N, Nakamura R, Hirose Y, Murosaki S, Yamamoto Y, et al. (2009) Oral administration of heat-killed *Lactobacillus plantarum* L-137 enhances protection against influenza virus infection by stimulation of type I interferon production in mice. Int Immunopharmacol 9: 1122-1125.
8. Kobayashi N, Saito T, Uematsu T, Kishi K, Toba M, et al. (2011) Oral administration of heat-killed *Lactobacillus pentosus* strain b240 augments protection against influenza virus infection in mice. Int Immunopharmacol 11: 199-203.
9. Zhanga W, Azevedoa MSP, Wenb K, Gonzaleza A, Saifa LJ, et al. (2008) Probiotic *Lactobacillus acidophilus* enhances the immunogenicity of an oral rotavirus vaccine in gnotobiotic pigs. Vaccine 26: 3655-3661.

10. Davidson LE, Fiorino A-M, Snydman DR, Hibberd PL (2011) Lactobacillus GG as an immune adjuvant for live attenuated influenza vaccine in healthy adults: a randomized double blind placebo controlled trial. Eur J Clin Nutr 65: 501-507.

11. Boge T, Rémigy M, Vaudaine S, Tanguyc J, Bourdet-Sicardc R, et al. (2009) A probiotic fermented dairy drink improves antibody response to influenza vaccination in the elderly in two randomised controlled trials. Vaccine 27: 5677-5684.

12. Yuji N, Takayuki I, Fumi I, Toshihiro M, Hiroshi S, et al. (2008) Antiallergic effects of *Lactobacillus pentosus* strain S-PT84 mediated by modulation of Th1/Th2 immunobalance and induction of IL-10 production. Int Arch Allergy Immunol 145: 249-257.

13. Izumo T, Maekawa T, Ida M, Kishi A, Akatani K, et al. (2011) Effect of *Lactobacillus pentosus* S-PT84 ingestion on IFN-α production from plasmacytoid dendritic cells by virus stimulation. Biosci Biotechnol Biochem 75: 370-372.

14. Izumo T, Maekawa T, Ida M, Noguchi A, Kitagawa Y, et al. (2010) Effect of intranasal administration of *Lactobacillus pentosus* S-PT84 on influenza virus infection in mice. Int Immunopharmacol 10: 1101-1106.

15. Nishino M, Mizuno D, Kimoto T, Shinahara W, Fukuta A, et al. (2009) Influenza vaccine with surfacten, a modified pulmonary surfactant, induces systemic and mucosal immune responses without side effects in minipigs. Vaccine 27: 5620-5627.

16. Koizumi S, Wakita D, Sato T, Mitamura R, Izumo T, et al. (2008) Essential role of Toll-like receptors for dendritic cell and NK1.1(+) cell-dependent activation of type 1 immunity by *Lactobacillus pentosus* strain S-PT84. Immunol Lett 120: 14-19.

17. Izumo T, Izumi f, Nakagawa I, Kitagawa Y, Sibata H, et al. (2011) Influence of *Lactobacillus pentosus* S-PT84 ingestion on the mucosal immunity of healthy and *Salmonella* typhimurium-infected mice. Biosci Microflora 30: 27-35.

18. Kimoto T, Mizuno D, Takei T, Kunimi T, Ono S, et al. (2013) Intranasal influenza vaccination using a new synthetic mucosal adjuvant SF-10: induction of potent local and systemic immunity with balanced Th1 and Th2 responses. Influenza Other Respir Viruses 7: 1218-1226.

19. Lin HT, Chuang CC, Wu HL, Chu DM, Wang YC (2013) Characterization of cross protection of Swine-Origin Influenza Virus (S-OIV) H1N1 and reassortant H5N1 influenza vaccine in BALB/c mice given a single-dose vaccination. J Biomed Sci 20: 19.

20. Goodwin K, Viboud C, Simonsen L (2006) Antibody response to influenza vaccination in the elderly: A quantitative review. Vaccine 24: 1159-1169.

Influenza A virus infection of vascular endothelial cells induces GSK-3β-mediated β-catenin degradation in adherens junctions, with a resultant increase in membrane permeability

M. Hiyoshi, I. L. Indalao, M. Yano, K. Yamane, E. Takahashi & H. Kido

Archives of Virology
Official Journal of the Virology Division of the International Union of Microbiological Societies

ISSN 0304-8608
Volume 160
Number 1

Arch Virol (2015) 160:225-234
DOI 10.1007/s00705-014-2270-5

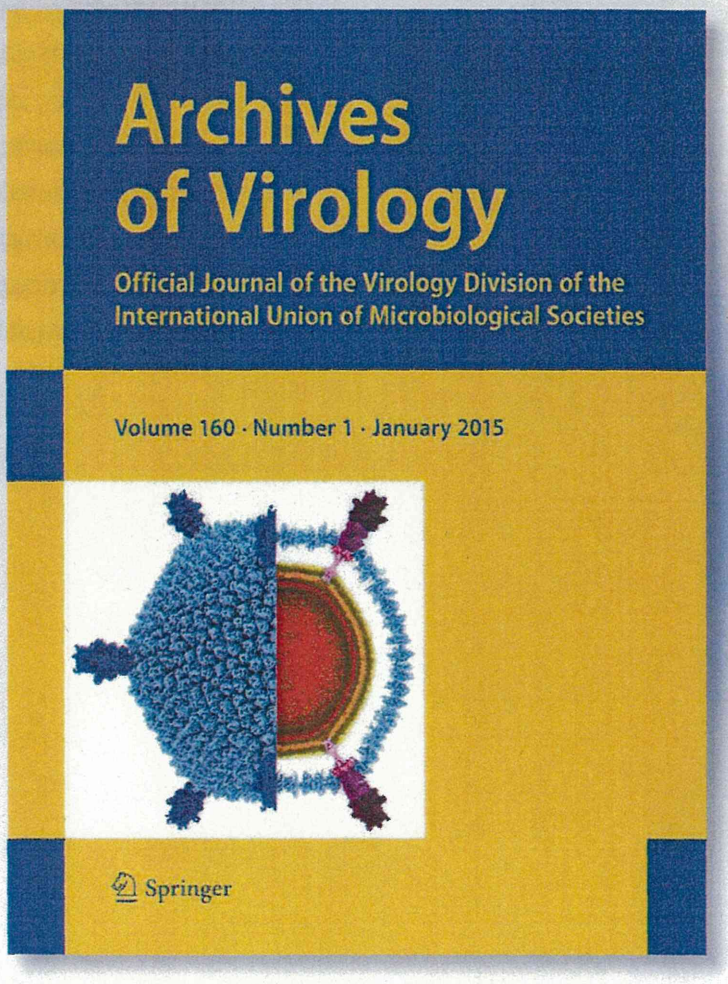

Springer

Arch Virol (2015) 160:225–234
DOI 10.1007/s00705-014-2270-5

ORIGINAL ARTICLE

Influenza A virus infection of vascular endothelial cells induces GSK-3β-mediated β-catenin degradation in adherens junctions, with a resultant increase in membrane permeability

M. Hiyoshi · I. L. Indalao · M. Yano · K. Yamane · E. Takahashi · H. Kido

Received: 25 June 2014 / Accepted: 25 October 2014 / Published online: 12 November 2014

Abstract Multiorgan failure with vascular hyperpermeability is the final outcome in the progression of seasonal influenza virus pneumonia and influenza-associated encephalopathy, and it is also common in infection with highly pathogenic avian influenza virus. However, the precise molecular mechanism by which influenza virus infection causes vascular endothelial cell hyperpermeability remains poorly defined. We investigated the mechanisms of hyperpermeability of human umbilical vein endothelial cells infected with influenza A virus (IAV)/Puerto Rico/8/34 (PR8) (H1N1). The levels of β-catenin, a key regulatory component of the vascular endothelial-cadherin cell adhesion complex, were markedly decreased during infection for 28 h, with increments of vascular hyperpermeability measured by transendothelial electrical resistance. Lactacystin (at 2 μM), a proteasome inhibitor, inhibited the decrease in β-catenin levels. Since the N-terminal phosphorylation of β-catenin by glycogen synthase kinase (GSK)-3β is the initiation step of proteasome-dependent degradation, we examined the effects of GSK-3β suppression by RNA interference in endothelial cells. IAV-infection-induced β-catenin degradation was significantly inhibited in GSK-3β-knockdown cells, and transfection of cells with recombinant β-catenin significantly suppressed IAV-induced hyperpermeability. These findings suggest that IAV infection induces GSK-3β-mediated β-catenin degradation in the adherens junctional complexes and induces vascular hyperpermeability. The *in vitro* findings of β-catenin degradation and activation of GSK-3β after IAV infection were confirmed in lungs of mice infected with IAV PR8 during the course of infection from day 0 to day 6. These results suggest that GSK-3β-mediated β-catenin degradation in adherens junctions is one of the key mechanisms of vascular hyperpermeability in severe influenza.

Introduction

Influenza A virus (IAV) is the most common infectious pathogen in humans and causes significant morbidity and mortality, particularly in infants and the elderly population [1, 2]. Multiorgan failure (MOF) with vascular hyperpermeability is reported in the progressive stage of seasonal influenza virus pneumonia, particularly in patients with underlying risk factors [3], and is also common in infections caused by highly pathogenic avian influenza virus [4]. Vascular hyperpermeability caused by destruction of a tight junction constituent, zonula occludens-1 (ZO)-1, of the blood-brain-barrier (BBB) in brain endothelial cells is also reported in influenza-associated encephalopathy in infancy and early childhood in East Asians [5–8]. We reported previously that the "influenza–cytokine–trypsin and matrix metalloprotease-9" cycle is a key pathogenic

M. Hiyoshi, I. L. Indalao and M. Yano contributed equally to this work.

M. Hiyoshi · I. L. Indalao · M. Yano · K. Yamane · E. Takahashi · H. Kido (✉)
Division of Enzyme Chemistry, Institute for Enzyme Research, The University of Tokushima, Kuramoto-cho 3-18-15, Tokushima 770-8503, Japan
e-mail: kido@tokushima-u.ac.jp

Present Address:
M. Hiyoshi
Department of Biochemistry, Shimane University Faculty of Medicine, Izumo, Shimane 693-8501, Japan

Present Address:
M. Yano
Department of Nutrition, School of Human Cultures, The University of Shiga Prefecture, Hikone, Shiga 522-8533, Japan

mechanism in the interaction between IAV infection and vascular endothelial cells and their hyperpermeability in severe influenza [8, 9].

The state of hypercytokinemia in IAV infection (e.g., high levels of tumor necrosis factor, interleukin 6, and interleukin-1β), called a "cytokine storm", affects cell adhesion, permeability, apoptosis, and mitochondrial energy metabolism and reactive oxygen species, potentially resulting in vascular dysfunction, hyperpermeability and MOF [10, 11], although their precise mechanisms have not been elucidated so far. Furthermore, IAV infection induces upregulation of trypsin and matrix metalloprotease-9 through an "influenza–cytokine–protease" cycle in various organs and vascular endothelial cells [8, 9, 11, 12], and an increase in the levels of these proteases in the extracellular space caused by this cycle results in the degradation of vascular basement membranes and the extracellular matrix, resulting in vascular hyperpermeability and inflammatory cell migration. Trypsin promotes viral entry and replication because IAV does not encode a viral hemagglutinin processing protease in its own genes, and post-transcriptional hemagglutinin cleavage by cellular trypsin-type proteases is needed for membrane fusion activity, virus entry into cells, and multiple cycles of viral replication [13–15]. In addition, trypsin evokes cytokine release via the proteinase-activated receptor (PAR)-2 [16] and also plays a role in BBB destruction by increasing intracellular calcium concentrations ($[Ca^{2+}]_i$) and loss of tight-junction protein ZO-1 via PAR-2 in the BBB [8, 17].

For the control of vascular permeability, there is another major type of cell-to-cell junction, the adherens junction, which is ubiquitously distributed along the vascular tree and is expressed in both blood and lymphatic vessels [18]. The adherens junction is formed by the transmembrane adhesion molecule vascular endothelial (VE)-cadherin and its cytoplasmic tail binding molecules, β-catenin and plakoglobin, which anchor to actin via α-catenin and stabilize the junction [19].

In this study, we investigated the mechanisms of IAV-induced disruption of adherens junctions and vascular hyperpermeability in human endothelial cells *in vitro* and confirmed these findings *in vivo*. We found that GSK-3β-mediated β-catenin degradation in the VE-cadherin complex in the adherens junction of human endothelial cells was associated with increased hyperpermeability after IAV infection.

Materials and methods

Cell culture

Normal human umbilical vein endothelial cells (HUVECs) (Kurabo Industries, Osaka, Japan) on type-I-collagen-coated dishes (10 cm diameter) were grown in HuMedia-EG2 culture medium using the protocol supplied by the manufacturer. The cells were cultured in a humidified atmosphere of 5 % CO_2–95 % air gas mixture at 37 °C.

Influenza A virus infection

IAV/PR/8/34 (H1N1) was provided by the Research Foundation for Microbial Diseases of Osaka University (Kagawa, Japan). Before infection of HUVEC with IAV PR8, the culture medium was replaced with serum-free HuMedia-EB2 infection medium containing 0.1 % bovine serum albumin (BSA). The cells were infected with IAV PR8 at a multiplicity of infection (MOI) of 1. After incubation for 1 h, the infection medium was replaced with a culture medium containing various reagents, and the cells were incubated for another 28 h.

For animal experiments, specified-pathogen-free 4-week-old weanling C57BL/6CrSlc female mice were obtained from Japan SLC and maintained in a 12-h light/dark cycle in a temperature-controlled room with free access to food and water. All animals were treated according to the Guide for the Care and Use of Laboratory Animals (NIH Publication No. 85-23, 1996), and the study was approved by the Animal Care Committee of the University of Tokushima. Under ketamine and xylazine anesthesia, 100 plaque-forming units of IAV PR8 in 20 μL of saline or saline alone as an uninfected control was instilled intranasally in mice. Body weight and survival were monitored daily, and the animals were assessed visually for signs of clinical disease including inactivity, ruffled fur, labored respiration and huddling behavior. Mice that lost ≥30 % of their original body weight and/or displayed evidence of pneumonia were sacrificed by overdose of intraperitoneal ketamine and xylazine. These experiments were conducted under animal BSL2 conditions.

Western immunoblotting

HUVECs after various treatments were lysed in radioimmunoprecipitation assay (RIPA) buffer (50 mM Tris-HCl, pH 8.0, 150 mM NaCl, 10 % glycerol, 1 % NP 40, 0.5 % deoxycholate, 0.4 mM EDTA, and 0.5 mM sodium orthovanadate) for 30 min at 4 °C. Mouse lungs isolated during the course of IAV infection (from day 0 to day 6) were homogenized with five volumes of RIPA buffer. Cell lysate and lung homogenate were centrifugation at 10,000×*g* for 30 min. The prepared cell lysates (20 μg protein/lane) and lung extracts (20 μg protein/lane) were separated by sodium dodecyl sulfate polyacrylamide gel electrophoresis (SDS-PAGE) using 10-to-20 % gradient gel and transferred onto an Immobilon-P membrane (Millipore, Bedford, MA). After blocking with 5 % non-fat milk in 20 mM

Tris-HCl, pH 7.5, 150 mM NaCl and 0.05 % Tween 20, the membranes were incubated with optimal primary antibodies for 2 h. The primary antibodies included anti-β-catenin, anti-VE-cadherin, anti-β-actin and anti-glycogen synthase kinase (GSK)-3β (all from Santa Cruz Biotechnology, Santa Cruz, CA), anti-phospho-GSK-3β (Ser9) (Cell Signaling Technology, Beverly, MA) and anti-IAV (Takara). Thereafter, peroxidase-conjugated anti-mouse (Invitrogen, Carlsbad, CA), -rabbit (Sigma, St. Louis, MO) or -goat (Sigma) IgG antibodies were incubated for 30 min, followed by enhanced chemiluminescence reagents (GE Healthcare Biosciences, Uppsala, Sweden) for 1 min.

Reverse transcription polymerase chain reaction (RT-PCR)

Total RNA was extracted from HUVECs using an RNeasy Mini Kit (QIAGEN, Hilden, Germany). RT-PCR was carried out using a One-Step RT-PCR Kit (QIAGEN) according to the instructions provided by the manufacturer. To amplify the PCR product of β-catenin, the following primer pair was used (forward primer, 5′-TTTGGCTGAA CCATCACAGA-3′; and reverse primer, 5′-TGTTGAG CAAGGCAACCATT-3′). The products were examined by agarose gel electrophoresis after 25 cycles.

Relative quantitation analysis

Protein or mRNA bands detected on X-ray films or pictures were calculated by densitometric analysis using Just TLC (Sweday, Lund, Sweden). The relative levels of the immunoblot or RT-PCR bands were expressed as mean values ±SD.

RNA interference

The sequence of the sense strand used to generate specific siRNA was obtained as follows: GSK-3β, NCBI Reference Sequence: NG_012922.1, 5′-AAATCTCTTGTCCTGCA ATAC-3′. A small interfering RNA (siRNA) was synthesized using a Silencer siRNA Construction Kit (Ambion, Austin, TX) according to the instructions supplied by the manufacturer. HUVECs were transfected with the siRNA at 10 nM, using Oligofectamine Transfection Reagent (Invitrogen) and grown for 72 h to allow sufficient decrease in the expression of this molecule.

Assessment of hyperpermeability by trans-endothelial electrical resistance (TEER) and transfection with recombinant β-catenin

HUVEC were plated in the upper chamber of type I collagen-coated cell culture inserts with a membrane of 3.0 μm pore size. After infection of the cells with IAV PR8 at a MOI of 1 for 24 h, some of the cells on the plates were transfected with recombinant β-catenin (1.2 μg/mL) (Millipore). Recombinant β-catenin was exposed to the transfection reagent TransIT-LT1 polyamine (Mirus, Madison, WI) for 15 min before transfection. After transfection for 4 h, the TEER across monolayers of endothelial cells was measured using Millicell-ERS (Millipore) using the method described previously [20, 21]. The electrical resistance of blank inserts containing the medium only was subtracted from the TEER measurements made from inserts containing confluent endothelial cell monolayers.

Statistical analysis

The mean values ±SD of individual groups were calculated, and the differences between groups were analyzed using the unpaired *t*-test or multiple comparisons (Bonferroni or Dunnett tests) after one-way analysis of variance (ANOVA). All statistical analyses were performed using Microsoft Excel (Microsoft, Redmond, WA) add-in Ekuseru-Toukei 2010 version 1.10 (Social Survey Research Information Co.). All values are two-tailed and those less than 0.05 were considered statistically significant.

Results

IAV infection downregulates β-catenin significantly, but not VE-cadherin, in adherens junctional proteins in HUVECs

Figures 1A and B show the results of immunoblotting analyses of β-catenin and VE-cadherin, the major adherens junctional proteins, in HUVECs infected with IAV PR8 at an MOI of 1 for 28 h or in uninfected cells. Infection significantly suppressed the expression of β-catenin to 24 % of the no-infection control ($P < 0.0001$). The expression of the transmembrane adhesive component VE-cadherin also tended to decrease, though not significantly, after infection ($P = 0.2472$). Quantitative RT-PCR analysis showed a slight, but significant, decrease in the β-catenin mRNA level to 84 % of the no-infection control ($P = 0.0188$) in infected HUVECs (Fig. 1C and D). The discrepancy between the suppression levels of β-catenin protein and those of β-catenin mRNA after IAV infection indicates that the marked suppression of the β-catenin protein level was probably due to enhanced β-catenin protein degradation.

Lactacystin inhibits IAV-induced β-catenin degradation

To verify the above-stated findings, HUVECs were treated with 2 μM lactacystin (Sigma), a proteasome inhibitor

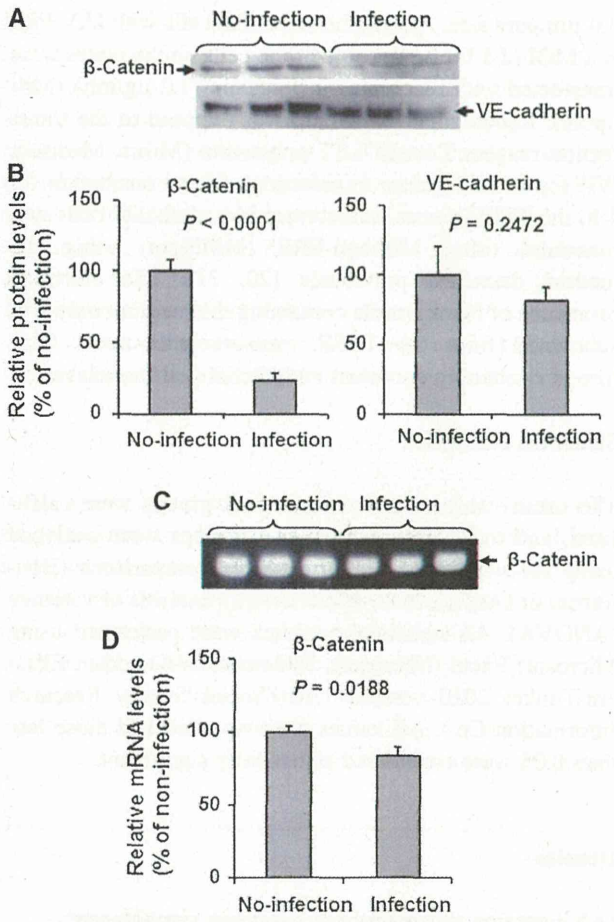

Fig. 1 Infection with IAV reduces the expression of β-catenin in adherens junctional proteins in HUVECs. **A.** Representative immunoblot (from three separate experiments) of β-catenin and VE-cadherin in cell lysates (20 μg protein/lane) of HUVECs after infection for 28 h with or without IAV PR8. As a control, saline was used as no-infection agent. **B.** Relative levels of β-catenin and VE-cadherin in the blot in panel A (n = 3), determined as described in Materials and methods. Statistical analysis was performed using the unpaired *t*-test. **C.** Representative RT-PCR data of β-catenin in control (uninfected) and IAV-infected HUVECs at 28 h post-transfection. D: Relative levels of β-catenin in the RT-PCR experiment shown in panel C (n = 3). Statistical analyses were conducted using the unpaired *t*-test

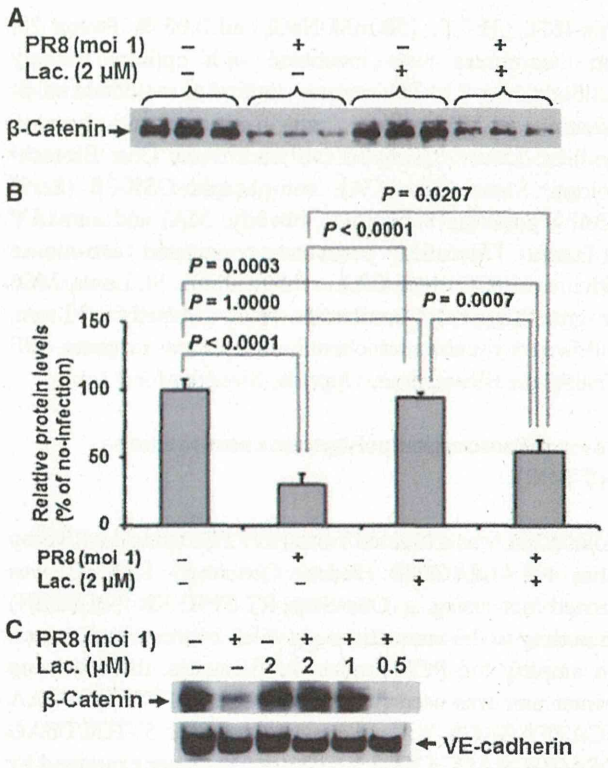

Fig. 2 *Lactacystin inhibits IAV-induced β-catenin suppression.* **A.** Representative immunoblot (from three separate experiments) of β-catenin in cell lysates (20 μg protein/lane) of control (uninfected) or IAV-infected HUVECs treated with or without lactacystin for 28 h. **B.** Relative level of β-catenin in the blot in panel A (n = 3). Multiple comparisons tests (Bonferroni test after one-way analysis of variance (ANOVA) were used for statistical analysis. **C.** Dose-response effect of lactacystin on β-catenin and VE-cadherin expression. HUVECs were treated with various concentrations of lactacystin (from 0 to 2 μM) at the time of infection and then incubated for 28 h. A representative immunoblot of β-catenin and VE-cadherin in cell lysates (20 μg protein/lane) with or without infection is shown

[22], at the time of PR8 infection and the cells were incubated for 28 h. Under no-infection conditions, lactacystin did not affect β-catenin protein levels in HUVEC ($P = 1.0000$) (Fig. 2A and B). In contrast, lactacystin significantly abrogated the suppression of the β-catenin protein level in IAV PR8-infected HUVECs ($P = 0.0207$), and the levels were 1.8-fold higher than those in infected cells that were not treated with lactacystin. The inhibitory effect of lactacystin was dose-dependent, and lactacystin at 0.5 μM was not enough to restore the β-catenin levels (Fig. 2C). Expression of VE-cadherin was not affected by treatment with various doses of lactacystin. These results confirmed that the downregulation of the β-catenin protein level in IAV PR8-infected HUVECs is the result of enhanced proteasomal degradation.

IAV PR8 infection activates GSK-3β in HUVECs

β-Catenin, which is phosphorylated by GSK-3β at residues 37 and 33, is recognized by the β-TrCP E3-ligase complex, ubiquitylated, and rapidly degraded by the 26S proteasome [23, 24]. To elucidate the mechanism(s) of enhanced β-catenin degradation in HUVEC by IAV infection, the expression level of the active form of dephosphorylated GSK-3β (Ser9) was analyzed by western immunoblotting using specific antibodies against GSK-3β and phospho-GSK-3β (Ser9) to detect the inactive form of phosphorylated GSK-3β (Fig. 3A and B). The total amount of GSK-3β in IAV PR8-infected cells was only

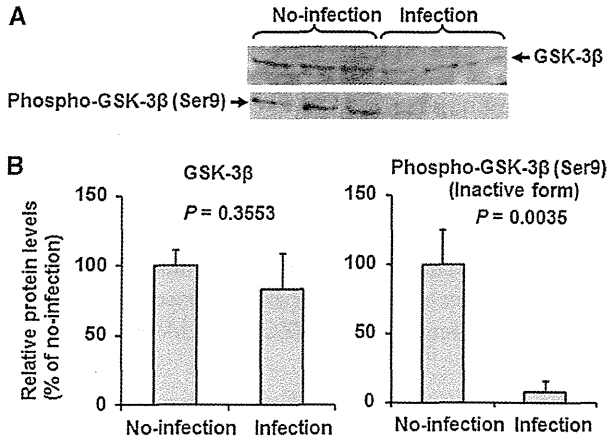

Fig. 3 IAV infection induces suppression of phosphorylated GSK-3β in HUVECs. **A.** Representative immunoblots (from three separate experiments) of total GSK-3β and phosphor-GSK-3β (Ser9) in cell lysates (20 μg protein/lane) of control (uninfected) or IAV-infected HUVECs. **B.** Relative levels of total GSK-3β and phosphor-GSK-3β (Ser9) in the blot in panel A (n = 3). Data are mean ± SD. Statistical analyses were conducted using the unpaired *t*-test

slightly decreased to 83 % of the no-infection control cells, and the decrease was not significant ($P = 0.3553$). In contrast, IAV infection markedly decreased the level of the phosphorylated-GSK-3β (Ser9) form to 8 % ($P = 0.0035$). These results indicate that IAV infection induces GSK-3β in HUVECs from the inactive phosphorylated-GSK-3β (Ser9) form to the active dephosphorylated-GSK-3β (Ser9) form.

GSK-3β knockdown protects against IAV infection-induced suppression of β-catenin expression

Since degradation of β-catenin, a major component of the VE-cadherin complex, is initiated by the activation of GSK-3β, we next analyzed the effects of GSK-3β gene-silencing on the level of β-catenin in IAV-infected and uninfected HUVECs (Fig. 4A and B). HUVECs treated with or without GSK-3β knockdown were infected with IAV PR8 at a MOI of 1 and β-catenin levels in the cells were measured by western immunoblotting at 28 h post-infection. Under no-infection conditions, GSK-3β knockdown treatment resulted in suppression of GSK-3β expression in HUVEC to about 20 % of the level without treatment. Although GSK-3β expression was downregulated in HUVECs by IAV infection, the expression was further suppressed by GSK-3β gene silencing to an undetectable level. The β-catenin expression level in HUVECs treated with GSK-3β knockdown under no-infection conditions was 76 % of those without knockdown treatment ($P = 0.0126$). However, the β-catenin expression level in GSK-3β knockdown cells was 1.9-fold of that in HUVECs

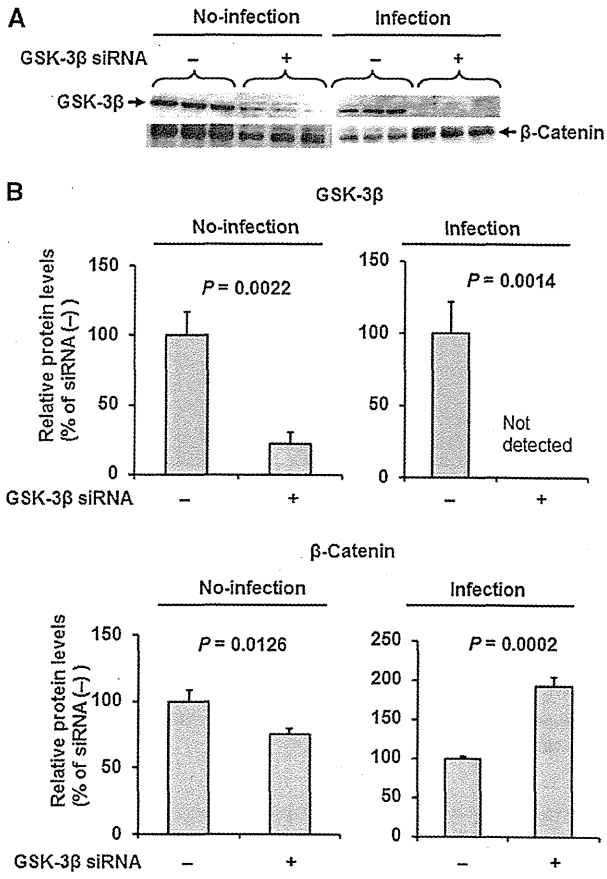

Fig. 4 GSK-3β knockdown protects against IAV-induced suppression of β-catenin. **A.** Representative immunoblots (from three separate experiments) of GSK-3β and β-catenin in cell lysates (20 μg protein/lane) of HUVECs pre-treated with or without GSK-3β knockdown under control (no-infection) and IAV-infection conditions. **B.** Relative levels of GSK-3β and β-catenin in the bolt in panel A (n = 3). Differences between groups were analyzed using the unpaired *t*-test

without treatment under infection conditions ($P = 0.0002$). These data suggest that the β-catenin level in the VE-cadherin complex is strictly regulated by GSK-3β in IAV-infected HUVECs.

Transfection with β-catenin restores the IAV-infection-disrupted barrier function

The hyperpermeability of monolayers of HUVECs was measured by TEER. Infection of HUVECs with IAV PR8 at an MOI of 1 for 24 h resulted in a significant decrease in TEER ($P = 0.0367$), indicating cell hyperpermeability (Fig. 5). Transfection of the vehicle (TransIT-LT1 polyamine) tended to reduce TEER, albeit insignificantly ($P = 0.5409$). However, pretreatment of HUVECs by transfection with recombinant β-catenin for 4 h markedly increased TEER ($P = 0.0003$), and the monolayer

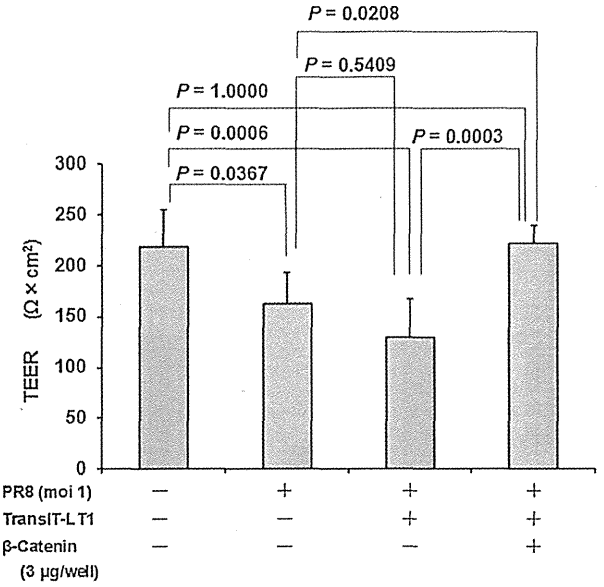

Fig. 5 Transfection with recombinant β-catenin abrogates IAV infection-induced impairment of barrier function. TEER data across monolayers of control (uninfected) and IAV-infected HUVECs (n = 6), and with or without recombinant β-catenin transfection were analyzed using multiple comparison (Bonferroni test) after one-way analysis of variance (ANOVA)

permeability was almost completely restored to the levels recorded in uninfected and untransfected cells.

Changes in expression levels of adherens junctional proteins and GSK-3β in lungs of mice infected with IAV PR8

The time courses of change in β-catenin, VE-cadherin, GSK-3β, phospho-GSK-3β (Ser 9) and viral nucleoprotein (NP) expression levels were analyzed in the lungs of mice infected intranasally with IAV PR8 at 100 PFU from day 0 to day 6. The average body weight of infected mice started to fall at day 3 postinfection and an approximately 26 % loss relative to the original weight was observed on day 6, but the average body weight of uninfected mice showed a continuous increase (Fig. 6A1). All animals survived during the experimental period except one infected animal, which died on day 6.

The viral NP levels in the lungs monitored by western immunoblotting showed that they started to increase at day 2 postinfection, reaching a peak at day 3 and then gradually decreasing (Fig. 6A2). Progressive and marked downregulation of β-catenin was noted during the infection period from day 2 to day 6 (Fig. 6B and C). This was coupled with simultaneous downregulation of phosphor-GSK-3β (Ser 9) (inactive form) expression in the lungs, and marked downregulation began at day 1 postinfection and persisted until day 6 postinfection. In contrast to these changes, total GSK-3β expression was steady until day 4 postinfection and was significantly upregulated at day 6. A mild and continuous decrease in the expression of VE-cadherin was detected until day 3 post-expression, followed by a marked decrease in expression from day 4 to day 6 postinfection. Changes in these expression levels were observed in the lungs at day 6 postinfection, the starting point of an obvious multi-organ failure phase with vascular hyperpermeability [15]. These *in vivo* changes in lung tissue added support to the *in vitro* findings of increased hyperpermeability after infection of HUVECs with IAV PR8.

Discussion

The present study resulted in several new findings: (i) IAV PR8 infection markedly decreased the level of a regulatory component of the VE-cadherin cell adhesion complex, β-catenin, in association with enhanced permeability of human vascular endothelial cells. (ii) The decrease in β-catenin protein levels in the cells was the result of degradation by activation of GSK-3β, and the degradation was inhibited by lactacystin, a proteasome inhibitor. (iii) IAV infection-induced β-catenin degradation was suppressed in HUVECs by GSK-3β knockdown and restoration of cellular barrier function by transfection with β-catenin. (iv) There was marked downregulation of adherens junctional protein β-catenin and upregulation of dephosphorylated GSK-3β (active GSK-3β) in the lungs of mice infected with IAV PR8.

Until recently, anti-influenza agents that inhibit viral replication have represented the best treatment option. However, MOF appears just after influenza virus peak proliferation with the initiation of host immune responses and development of metabolic disorders [11, 15], and thus the use of antiviral neuraminidase inhibitors is not suitable for the treatment of MOF after viral proliferation. MOF induced by severe IAV infection is the final outcome of circulatory failure, hypoxemia, and vascular hyperpermeability of endothelial cells through the "influenza–cytokine–trypsin and matrix metalloprotease-9" cycle [8, 11], with disruption of vascular junctions. In a series of studies, we reported previously that upregulation of trypsin in brain vascular endothelial cells by pro-inflammatory cytokines after IAV infection plays a pivotal role in the destruction of tight junctions in the BBB through an increase in $[Ca^{2+}]_i$ and loss of ZO-1 via proteinase-activated receptor-2 signaling [8, 17].

Adherens junction, another major type of junction in the vascular endothelium, plays important roles in contact inhibition of endothelial cell growth and paracellular permeability to circulating leukocytes and solutes. Adherens junctions are ubiquitously distributed, and endothelial cells

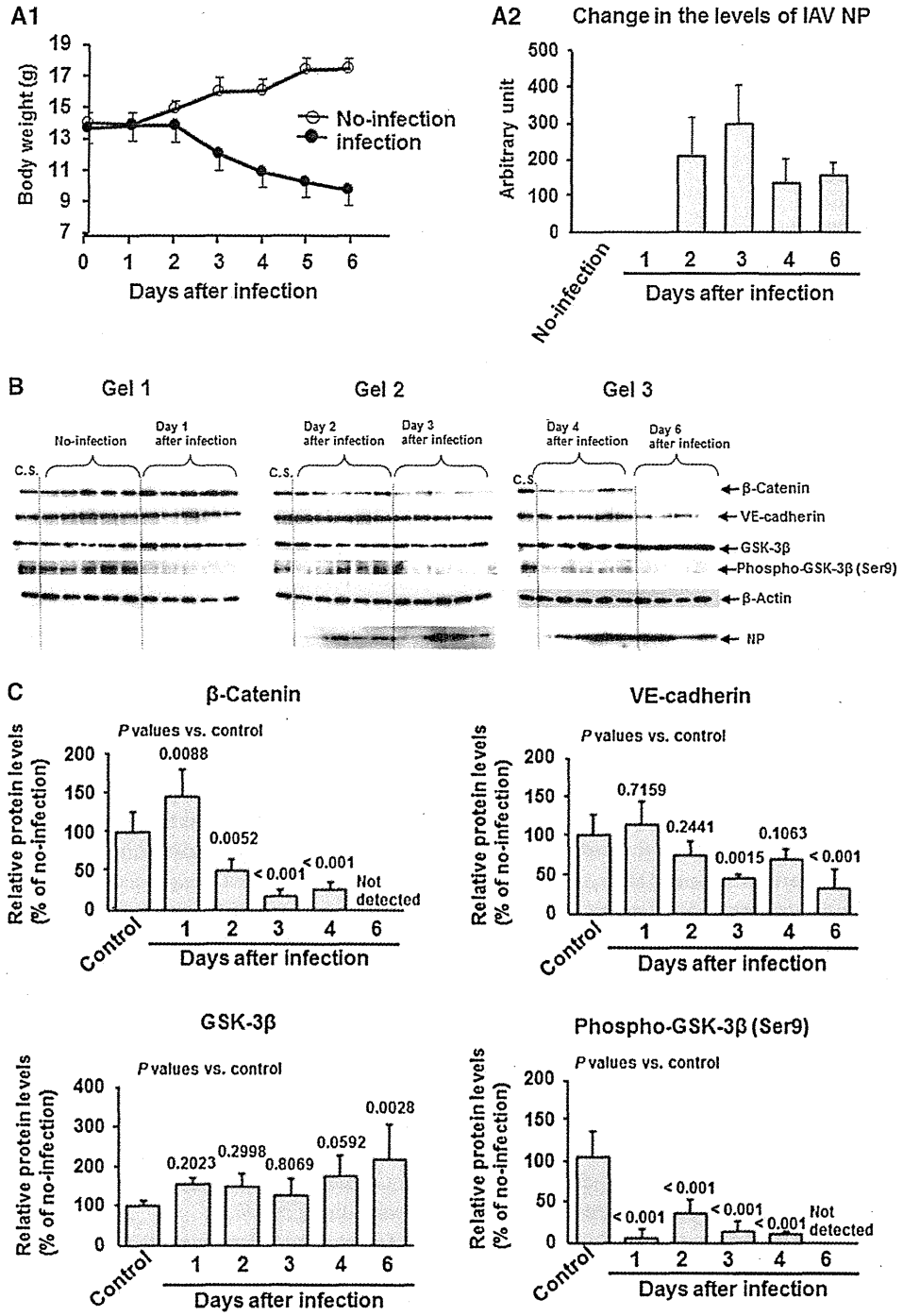

Fig. 6 β-Catenin suppression and GSK-3β activation in lungs of IAV-infected mice. A1, change in body weight of infected and uninfected mice (five mice in each group). A2, change in viral NP levels in the lungs monitored by western immunoblotting (B). One infected animal died on day 6 postinfection. The values represent the mean ± SD of five or four mice. B and C, Data represent the expression levels (B) and relative quantified data (C) of β-catenin, VE-cadherin, GSK-3β, and phospho-GSK-3β (Ser9) in lung extracts (20 μg protein/lane) of control (no-infection) and IAV-infected mice from day 1 to day 6 postinfection. C.S., calibration standard (mixture of uninfected sample except for NP analysis) to normalize the intensity of protein bands in different gels. As the C.S. for NP, a sample from one animal after infection for 4 days was used. β-Actin was used as an internal control. Data are representative of three separate experiments. Multiple comparison (Dunnett test) after ANOVA were used for statistical analysis. *P*-values are relative to the control (no infection)

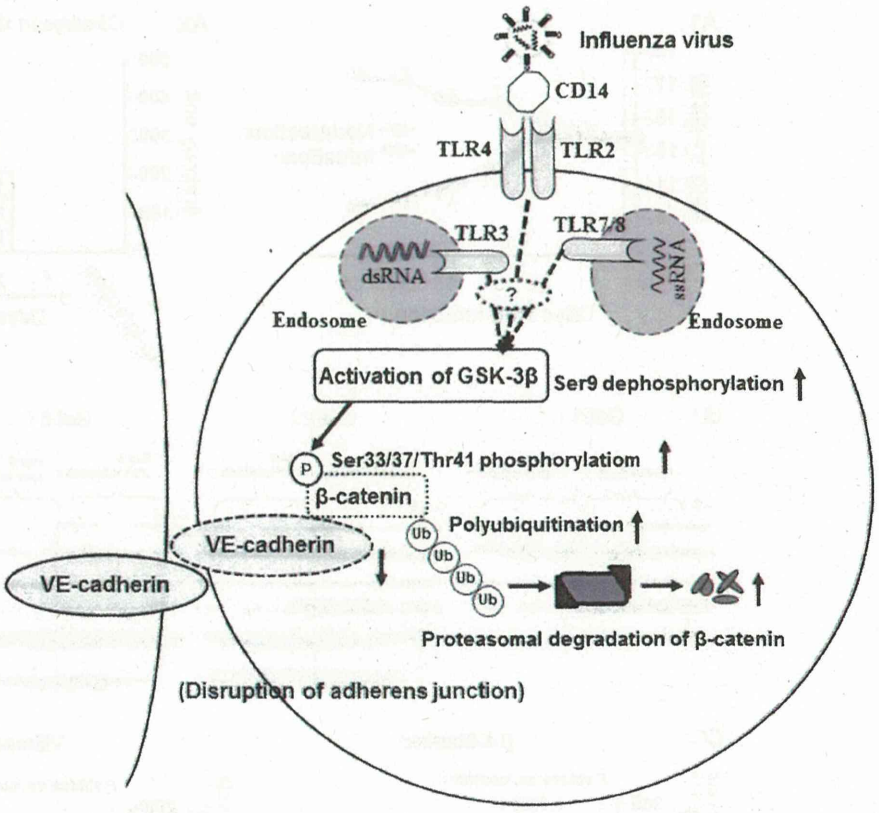

Fig. 7 Diagram illustrating the proposed mechanism of disruption of the adherens junctional complexes of vascular endothelial cells after severe IAV infection. Infection of vascular endothelial cells with IAV decreases β-catenin in the VE-cadherin-β-catenin adhesive complex by activation of GSK-3β and the phosphorylation-dependent ubiquitin-proteasome degradation pathway. TLR, Toll-like receptor; dsDNA, double-stranded DNA; ssRNA, single-stranded RNA. The question mark indicates that signal transductions between TLRs and GSK-3β are unidentified

in all types of blood vessels express VE-cadherin. The cytoplasmic tail of VE-cadherin binds β-catenin and plakoglobin at the carboxy-terminal region, both of which link α-catenin and anchor the complex to the actin cytoskeleton [18]. The first of these, β-catenin is a major regulatory component of the VE-cadherin-β-catenin adhesive complex, and its level is tightly regulated by GSK-3β, followed by the phosphorylation-dependent ubiquitin-proteasome degradation pathway in a manner similar to the phosphorylation-dependent degradation of IκB [23].

As an extension to our previous studies on the mechanisms of vascular hyperpermeability in MOF caused by severe IAV infection, we studied the mechanisms of destruction of the VE-cadherin-β-catenin adhesive complex and vascular hyperpermeability after IAV infection in human endothelial cells, both *in vitro* and *in vivo*. Our results showed marked β-catenin degradation by proteasomes and a significant decrease in phosphorylated GSK-3β (Ser9) expression in HUVECs after IAV infection (Figs. 1, 3 and 6). The findings of downregulation of β-catenin after IAV infection through the activation of GSK-3β followed by the phosphorylation-dependent ubiquitin-proteasome degradation pathway were supported by the experiments of GSK-3β gene silencing. GSK-3β-gene-silenced HUVECs showed almost complete protection against β-catenin downregulation in cells infected with IAV (Fig. 4), and β-catenin degradation was inhibited by lactacystin (Fig. 2). In addition, expression of recombinant β-catenin in HUVECs almost completely restored monolayer hyperpermeability induced by IAV infection. These results indicate that the level of β-catenin in the VE-cadherin-β-catenin adhesive complex is important for regulation of vascular permeability and that the β-catenin level is regulated by the GSK-3β-mediated β-catenin degradation pathway. The findings with IAV-infected HUVECs support previous studies on β-catenin degradation in the absence of Wingless/Wnt signaling pathway via GSK-3β-mediated β-catenin phosphorylation and the phosphorylation-dependent ubiquitin-proteasome degradation pathway in various mammalian cells [23].

The mitochondria-mediated caspase activation pathway is a major apoptotic pathway characterized by mitochondrial outer membrane permeabilization [24], and degradation of β-catenin by caspase-3 in the signaling pathway of apoptosis is another major contributing factor to tissue and cell damage, including hyperpermeability of endothelial cells [25–28]. We reported previously that IAV infection induces hyperpermeability associated with mitochondrial dysregulation, calcium mobilization, and loss of ZO-1 via protease-activated receptor in HUVECs [8] and apoptosis via mitochondrial membrane depolarization in cardiomyoblasts [9]. Upregulated TNF-α also induces mitochondrial

dysregulation through increasing mitochondrial O_2^- production and depleting ATP synthesis, decreasing oxygen consumption [10, 29], and increasing $[Ca^{2+}]_i$ [30].

GSK-3β is a serine/threonine protein kinase that has been shown recently to play a key role during the inflammatory response induced by various pathogenic bacteria, such as *Francisella tularensis*, the causative agent of highly virulent tularemia [31], *Burkholderia pseudomallei* [32] and group A streptococcus [33]. Bacterial lipopolysaccharides and lipid A are recognized by the Toll-like receptor (TLR)-2 on the cellular membrane and regulate GSK-3β activity via a phosphoinositide 3-kinase-Akt-dependent pathway [31]. In the present study, we found GSK-3β activation-mediated β-catenin degradation and monolayer hyperpermeability in IAV-infected HUVECs, and we propose a mechanism for the disruption of the adherens junctional complexes of vascular endothelial cells after severe IAV infection (Fig. 7). Since TLR2 and TLR4 bind to viral structural protein with CD14 [34], TLR7/8 binds to ssRNA and TLR3 binds to dsRNA [17], further studies on IAV-induced signal transduction from TLRs to GSK-3β activation are needed. In addition, there is also a need to design new therapeutic agents that can upregulate β-catenin and inhibit GSK-3β in vascular endothelial cells.

In summary, our results show that infection of HUVECs with IAV PR8 markedly decreases β-catenin levels in the VE-cadherin-β-catenin adhesive complex of HUVECs, together with hyperpermeability of HUVEC monolayers. The level of β-catenin in the adhesive complex is tightly regulated by activation of GSK-3β and the phosphorylation-dependent ubiquitin-proteasome degradation pathway. Destruction of the VE-cadherin-β-catenin adhesive complex could be one of the main pathomechanisms of MOF after severe IAV infection.

Acknowledgments The authors thank Dr. Junji Chida for stimulating discussion and comments. This research was funded in part by Grant-in-Aid 24249059 from the Ministry of Education, Culture, Sports, Science, and Technology of Japan and by a Health and Labor Sciences Research Grant (grant no. 12103307) from the Ministry of Health, Labor and Welfare of Japan.

References

1. Lipatov MS, Govorkova EA, Webby RJ, Ozaki H, Peiris M et al (2004) Influenza: emergence and control. J Virol 78:8951–8959. doi:10.1128/JVI.78.17.8951-8959.2004
2. Kim HW, Brandt CD, Arrobio JO, Murphy B, Chanock RM et al (1979) Influenza A and B virus infection in infants and young children during the years 1957-1976. Am J Epidemiol 109:464–479
3. Chowell G, Echevarria-Zuno S, Viboud C, Simonsen L, Miller MA et al (2012) Epidemiological characteristics and underlying risk factors for mortality during the autumn 2009 pandemic wave in Mexico. PLoS One 7(7):e41069. doi:10.1371/journal.pone.0041069
4. Perkins LE, Swayne DE (2001) Pathobiology of A/chicken/Hong Kong/220/97 (H5N1) avian influenza virus in seven gallinaceous species. Vet Pathol 38:149–164. doi:10.1354/vp.38-2-149
5. Delorme L, Middleton PL (1979) Influenza A virus associated with acute encephalopathy. Am J Dis Child 133:822–824. doi:10.1001/archpedi.1979.02130080062011
6. Yao D, Mizuguchi H, Yamaguchi M, Yamada H, Chida J et al (2008) Thermal instability of compound variants of carnitine palmitoyltransferase II and impaired mitochondrial fuel utilization in influenza-associated encephalopathy. Hum Mutat 29:718–727. doi:10.1002/humu.20717
7. Yao M, Yao D, Yamaguchi M, Chida J, Yao D et al (2011) Bezafibrate upregulates carnitine palmitoyltransferase II expression and promotes mitochondrial energy crisis dissipation in fibroblasts of patients with influenza-associated encephalopathy. Mol Genet Metab 104:265–272. doi:10.1016/j.ymgme.2011.07.009
8. Wang S, Le TQ, Kurihara N, Chida J, Cisse Y et al (2010) Influenza virus–cytokine–protease cycle in the pathogenesis of vascular hyperpermeability in severe influenza. J Infect Dis 202:991–1001. doi:10.1086/656044
9. Pan HY, Yamada H, Chida J, Wang S, Yano M et al (2011) Upregulation of ectopic trypsins in the myocardium by influenza A virus infection triggers acute myocarditis. Cardiovasc Res 58:19–28. doi:10.1093/cvr/cvq358
10. Spraque AH, Khalil RA (2009) Inflammatory cytokines in vascular dysfunction and vascular disease. Biochem Pharmacol 78:539–552. doi:10.1016/j.bcp.2009.04.029
11. Yamane K, Indalao IL, Chida J, Yamamoto Y, Hanawa M et al (2014) Diisopropylamine dichloroacetate, a novel pyruvate dehydrogenase kinase 4 inhibitor, as a potential therapeutic agent for metabolic disorders and multiorgan failure in severe influenza. PLoS One 9(5):e98032. doi:10.1371/journal.pone.0098032
12. Le TQ, Kawachi M, Yamada H, Shiota M, Okumura Y et al (2006) Identification of trypsin I as a candidate for influenza A virus and Sendai virus envelope glycoprotein processing protease in rat brain. Biol Chem 387:467–475. doi:10.1515/BC.2006.062
13. Klenk HD, Rott R, Orlich M, Blödom J (1975) Activation of influenza A viruses by trypsin treatment. Virology 68:426–439. doi:10.1016/0042-6822(75)90284-6
14. Kido H, Okumura Y, Yamada H, Le TQ, Yano M (2007) Proteases essential for human influenza virus entry into cells and their inhibitors as potential therapeutic agents. Curr Pharm Des 13:405–414. doi:10.2174/138161207780162971
15. Kido H, Okumura Y, Takahashi E, Pan HY, Wang S et al (2012) Role of host cellular proteases in the pathogenesis of influenza and influenza-induced multiple organ failure. Biochim Biophys Acta 1824:186–194. doi:10.1016/j.bbapap.2011.07.001
16. Niu QX, Chen HQ, Chen ZY, Fu YL, Lin JL et al (2008) Induction of inflammatory cytokine release from human umbilical vein endothelial cells by agonists of proteinase-activated receptor-2. Clin Exp Pharmacol Physiol 35:89–96. doi:10.1111/j.1440-1681.2007.04755.x
17. Pan HY, Yano M, Kido H (2011) Effects of inhibitors of Toll-like receptors, protease-activated receptor-2 signalings and trypsin on influenza A virus replication and upregulation of cellular factors in cardiomyocytes. J Med Invest 58:19–28. doi:10.2152/jmi.58.19
18. Bazzono G, Dejana E (2004) Endothelial cell-to-cell junctions: molecular organization and role in vascular homeostasis. Physiol Rev 84:869–901

19. Dejana E, Orsenigo F, Lampugnani MG (2008) The role of adherens junctions and VE-cadherin in the control of vascular permeability. J Cell Sci 121:2115–2122. doi:10.1242/jcs.017897
20. Nakamuta S, Endo H, Higashi Y, Kousaka A, Yamada H et al (2008) Human immunodeficiency virus type 1 gp120-mediated disruption of tight junction proteins by induction of proteasome-mediated degradation of zonula occludens-1 and -2 in human brain microvascular endothelial cells. J Neurovirol 14:186–195. doi:10.1080/13550280801993630
21. Dewi BE, Takasaki T, Kurane I (2008) Peripheral blood mononuclear cells increase the permeability of dengue virus-infected endothelial cells in association with downregulation of vascular endothelial cadherin. J Gen Virol 89:642–652. doi:10.1099/vir.0.83356-0
22. Liao CK, Jeng CJ, Wang HS, Wang SH, Wu JC (2013) Lipopolysaccharide induces degradation of connexin43 in rat astrocytes via the ubiquitin-proteasome proteolytic pathway. PLoS One 8(11):e79350. doi:10.1371/journal.pone.0079350
23. Aberle H, Bauer A, Stappert J, Kispert A, Kemler R (1997) β-Catenin is a target for the ubiquitin-proteasome pathway. EMBO J 16:3797–3804. doi:10.1093/emboj/16.13.3797
24. Xiong S, Mu T, Wang G, Jiang X (2014) Mitochondria-mediated apoptosis in mammals. Protein Cell. doi:10.1007/s13238-014-0089-1
25. Steinhusen U, Badock V, Bauer A, Behrens J, Wittman-Liebold B et al (2000) Apoptosis-induced cleavage of beta-catenin by caspase-3 results in proteolytic fragments with reduced transactivation potential. J Biol Chem 275:16345–16353. doi:10.1074/jbc.M001458200
26. Tran AT, Cortens JP, Du Q, Wilkins JA, Coombs KM (2013) Influenza virus induces apoptosis via BAD-mediated mitochondrial dysregulation. J Virol 87:1049–1060. doi:10.1128/JVI.02017-12
27. Childs EW, Tharakan B, Hunter FA, Tinsley JH, Cao X (2007) Apoptotic signaling induces hyperpermeability following hemorrhagic shock. Am J Physiol Heart Circ Physiol 292:H3179–H3189. doi:10.1152/ajpheart.01337.2006
28. Tharakan B, Hellman J, Sawant DA, Tinsley JH, Parrish AR et al (2012) β-Catenin dynamics in the regulation of microvascular endothelial cell hyperpermeability. Shock 37:306–311. doi:10.1097/SHK.0b013e318240b564
29. Mariappan N, Elks CM, Fink B, Francis J (2009) TNF-induced mitochondrial damage: a link between mitochondrial complex I activity and left ventricular dysfunction. Free Radic Biol Med 46:462–470. doi:10.1016/j.freeradbiomed.2008.10.049
30. Mizuguchi M, Yamanouchi H, Ichiyama T, Shiomi M (2007) Acute encephalopathy associated with influenza and other viral infection. Acta Neurol Scand 115:45–56. doi:10.1111/j.1600-0404.2007.00809.x
31. Zhang P, Katz J, Michalek SM (2009) Glycogen synthase kinase-3β (GSK3β) inhibition suppress the inflammatory response to *Francisella* infection and protects against tularemia in mice. Mol Immunol 46:677–687. doi:10.1016/j.molimm.2008.08.281
32. Tay TF, Maheran M, Too SL, Hasidah MS, Ismail G et al (2012) Glycogen synthase kinase-3β inhibition improved survivability of mice infected with *Burkholderia pseudomallei*. Trop Biomed 29:551–567
33. Chang YT, Chen CL, Lin CF, Lu SL, Cheng MH, Kuo CF, Lin YS (2013) Regulatory role of GSK-3β on NF-κB, nitric oxide, and TNF-α in group A streptococcal infection. Mediators Inflamm 2013:720689. doi:10.1155/2013/720689
34. Pauligk C, Nain M, Reiling N, Gemsa D, Kaufmann A (2004) CD14 is required for influenza A virus-induced cytokine and chemokine production. Immunobiology 209:3–10. doi:10.1016/j.imbio.2004.04.002

Am J Physiol Heart Circ Physiol 307: H922–H932, 2014.
First published July 18, 2014; doi:10.1152/ajpheart.00076.2014.

Ectopic trypsin in the myocardium promotes dilated cardiomyopathy after influenza A virus infection

Hai-Yan Pan,[1] Hua-Mei Sun,[1] Lu-Jing Xue,[1] Min Pan,[1] Yi-Ping Wang,[1] Hiroshi Kido,[2] and Jian-Hua Zhu[1]

[1]*Department of Cardiology, Affiliated Hospital of Nantong University, Institute of Cardiovascular Research, Nantong University, Jiangsu, China; and* [2]*Division of Enzyme Chemistry, Institute for Enzyme Research, The University of Tokushima, Tokushima, Japan*

Submitted 3 February 2014; accepted in final form 11 July 2014

Pan H, Sun H, Xue L, Pan M, Wang Y, Kido H, Zhu J. Ectopic trypsin in the myocardium promotes dilated cardiomyopathy after influenza A virus infection. *Am J Physiol Heart Circ Physiol* 307: H922–H932, 2014. First published July 18, 2014; doi:10.1152/ajpheart.00076.2014.—We have previously reported that ectopic trypsin in the myocardium triggers acute myocarditis after influenza A virus (IAV) infection. As myocarditis is a common precursor to dilated cardiomyopathy (DCM), the aim of the present study was to investigate the influence of trypsin on the progression of DCM after IAV infection. IAV-infected mice treated with saline or trypsin inhibitor were euthanized on *days 0, 9, 20, 40* and *60* postinfection. Trypsin expression colocalized with myocardial inflammatory loci and IAV-induced myocarditis peaked on *day 9* postinfection and alleviated by *day 20* but persisted until *day 60* postinfection, even though replication of IAV was not detected from *day 20* postinfection. Similar time courses were observed for the activation of pro-matrix metalloproteinase (pro-MMP)-9 and expression of the proinflammatory cytokines IL-6, IL-1β, and TNF-α. Degradation of collagen type I, proliferation of ventricular interstitial collagen, and expression of collagen type I and III mRNA increased significantly during acute and chronic phases; collagen type III mRNA increased more significantly than collagen type I mRNA. Cardiac function progressively deteriorated with progressive left ventricular dilation. The trypsin inhibitor aprotinin suppressed pro-MMP-9 activation and cytokine release, alleviated myocardial inflammation, and restored collagen metabolism during acute and chronic phases of myocarditis. This effectively prevented ventricular dilation and improved cardiac function. These results suggest that ectopic trypsin in the myocardium promoted DCM through chronic activation of pro-MMP-9, persistent induction of cytokines, and mediation of collagen remodeling. Pharmacological inhibition of trypsin activity might be a promising approach for the prevention of viral cardiomyopathy.

trypsin; myocarditis; dilated cardiomyopathy; influenza virus; extracellular matrix remodeling

THE INFLUENZA A VIRUS (IAV) is the most common infectious pathogen in humans. Acute myocarditis is a well-known complication of influenza infection and a common prelude to inflammatory dilated cardiomyopathy (DCM) that can lead to chronic heart failure (1, 49). A long-term followup study (18) in patients with acute myocarditis documented the development of DCM in 21% of patients over a mean followup period of 3 yr. The course of viral myocarditis has three distinct, successive stages: acute viral infection, immune cell infiltration, and cardiac remodeling (29). Although progress has been made in understanding the pathogenesis of DCM after viral infection, the precise mechanisms involved in the transition from viral myocarditis to DCM are not well understood.

During IAV infection, host factors such as proinflammatory cytokines, matrix metalloproteinases (MMPs), and ectopic trypsin are induced (39). Among these factors, ectopic trypsin, serving as a viral envelope hemagglutinin-processing protease, is crucial for viral entry, replication, and spread, because the IAV genome does not have a hemagglutinin-processing protease and hemagglutinin cleavage by cellular proteases at the posttranscriptional level is a prerequisite for membrane fusion activity (16). The expression profile of trypsin is likely a major determinant of IAV tissue tropism and pathogenicity. In addition, trypsin converts pro-MMPs to active MMPs (20, 39, 44) and promotes cytokine release through proteinase-activated receptor (PAR)-2 (35). Active MMPs, such as MMP-2 and MMP-9, degrade vascular basement membranes and the extracellular matrix (ECM), which could promote endothelial hyperpermeability and inflammatory cell migration (53). Degradation of the ECM could initiate anoikis in neighboring healthy tissue (31), leading to cardiac dilation and dysfunction. Furthermore, active MMP-2 and MMP-9 convert proinflammatory cytokines into their active forms (9, 28). Activated cytokines, such as TNF-α, IL-1β, and IL-6 recruit inflammatory cells and increase nitric oxide production in the heart (42) and promote cardiac remodeling via serpin A-3n (5). Overproduction of nitric oxide contributes to the development of DCM by inducing myocardial ATP depletion and cardiomyocyte apoptosis (14, 48).

The myocardial ECM is mainly composed of collagen type I (Col I; 85%) and Col type III (Col III; 11%) (8), which provide architectural support for cardiac myocytes and are important in myocardial function (41). Collagenases like MMP-9 and MMP-2 can remove collagen from struts and tethers, which are critical structures for preventing myocyte slippage (11, 23). Proinflammatory cytokines induce new collagen deposition, which can be misdirected to intercellular septa with a defective content of permanent cross-links (24). These effects can contribute to heart overextension and dilation.

We have previously reported that IAV-induced trypsin expression in the myocardium triggers acute viral myocarditis through stimulation of IAV replication, pro-MMP-9 activation, and cytokine induction (39). The aim of the present study was to clarify the role of trypsin in the progression of DCM after IAV infection. We defined the kinetics of trypsin upregulation during acute and chronic phases of myocarditis and investigated the effects of trypsin upregulation on the persistence of myocardial inflammation, changes in myocardial interstitial collagen components, and DCM development. The results

Address for reprint requests and other correspondence: J.-H. Zhu, Dept. of Cardiology, Affiliated Hospital of Nantong Univ., Institute of Cardiovascular Research, Nantong Univ., Jiangsu 226001, China (e-mail: dr.zhujianhua@gmail.com).

suggested that trypsin inhibition might prevent DCM with improved cardiac function after IAV infection.

METHODS

Influenza myocarditis model. This study conformed with Animal Research: Reporting In Vivo Experiments guidelines (17) and was approved by the Animal Care Committee of Nantong University. We randomly assigned 90 specific pathogen-free 8-wk-old male BALB/c mice (Comparative Medicine Center of Yangzhou University, Jiangsu, China) to a mock-infected group or to IAV-infected groups treated with saline or the trypsin inhibitor aprotinin (n = 10 mice/group). Under chloral hydrate anesthesia, mice were infected intranasally with 40 plaque-forming units of IAV/PR/8/34 (H1N1) (VR1469, American Type Culture Collection) in 15 μl saline or saline vehicle and euthanized on *days 0, 9, 20, 40,* or *60* postinfection. To analyze the effects of trypsin inhibition, aprotinin (Sigma-Aldrich Shanghai Trading, Shanghai, China) was injected intraperitoneally at 4 mg/kg daily until euthanasia.

Hemodynamic measurements. Transthoracic echocardiography was performed in mice using a VisualSonics vevo 770 ultrasonograph with a 30-MHz transducer (VisualSonics, Toronto, ON, Canada) under light anesthesia from an intramuscular injection of ketamine (30 mg/kg) before euthanasia. Left ventricular (LV) M-mode echocardiograms were obtained from a parasternal short-axis view. LV end-diastolic dimension (LVEDD), LV end-systolic dimension (LVESD), LV posterior wall thickness at end diastole (LVPWd), and LV posterior wall thickness at end systole (LVPWs) were recorded. Fractional shortening (FS) was calculated as follows: FS = (LVEDD − LVESD)/LVEDD × 100. LV end-diastolic volume (LVEDV) and LV end-systolic volume (LVESV) were measured from the parasternal long-axis view and calculated using Simpson's formula (4). Stroke volume (SV) and cardiac output (CO) were calculated by the following formulas: SV = LVEDV − LVESV and CO = SV × heart rate, respectively. LV ejection fraction (EF) was calculated as follows: EF = (SV/LVEDV) × 100. All parameters were measured from three consecutive cycles and averaged.

ELISA. Mouse blood was collected from the right ventricle after anesthesia. Plasma levels of Col I cross-linked carboxy-terminal telopeptide (ICTP) were measured with ELISA kits according to the recommendation of the manufacturer (Antibodies-online).

Tissue preparation. Isolated hearts were cut into halves with one portion fixed with 4% buffered paraformaldehyde solution for histopathological evaluation and the other portion stored at −80°C for biochemical analyses. All experiments were repeated at least three times.

Histopathological preparation. Tissues fixed in 4% paraformaldehyde were dehydrated in graded ethanol, embedded in paraffin, and sliced into 5-μm sections. After deparaffinization, sections were subjected to routine hematoxylin and eosin staining or van Gieson staining for the identification of collagen distribution.

Immunostaining. Immunohistochemistry for upregulated trypsin in the myocardium was performed as previously described (22, 39). Endogenous peroxidase activity was quenched with 3% H_2O_2 in methanol. Nonspecific binding sites were blocked with goat serum. Immune depositions in sections were detected with rabbit anti-trypsin antibody (Santa Cruz Biotechnology). Avidin-biotin-peroxidase kits (Vector Labs, Burlingame, CA) were used to visualize trypsin. For immunofluorescent staining, rabbit anti-trypsin (Santa Cruz Biotechnology) and mouse anti-IAV (Takara Bio, Shiga, Japan) were used as primary antibodies. Goat anti-rabbit IgG Texas red-conjugated antibody (Molecular Probes) and goat anti-mouse IgG FITC-conjugated antibody (Sigma-Aldrich) were used as secondary antibodies to visualize trypsin and IAV immunodeposits in hearts.

RT-PCR. Total RNA was extracted with TRIzol Reagent (Sangon Biotech, Shanghai, China), and 2 μg RNA was reverse transcribed with a TIANScript cDNA Synthesis kit (Tiangen Biotech, Beijing, China) for the synthesis of host and IAV cDNA. Trypsin, IAV nonstructural protein (NS)1, Col I, and Col III gene segments were amplified with a Taq PCR MasterMix kit (Tiangen Biotech) as previously described (15, 39). RT-PCR products were analyzed by agarose gel electrophoresis and visualized by treatment with ethidium bromide.

Immunoblot analysis and gelatin zymograph. Tissues were homogenized with three volumes of 0.05 M Tris·HCl (pH 7.6) containing 2% SDS and 0.5 M NaCl. Immunoblot analysis was performed as previously described (22). Target-specific antibodies were used to detect trypsin, MMP-9, MMP-2, TNF-α, IL-6, IL-1β, and actin (Santa Cruz Biotechnology). Immunoreactive bands were visualized by an enhanced chemiluminescence detection system (Cell Signaling Technology). MMP-2 and MMP-9 activities were analyzed by zymography. Protein extracts were separated by electrophoresis on 10% gelatin zymogram gels (Invitrogen) at 4°C. Gels were incubated in renaturing buffer (Invitrogen) at room temperature for 30 min and in developing buffer (Invitrogen) at 37°C for 4 h. Bands of gelatin degradation were visualized by staining with Coomassie brilliant blue R-250 and destaining as appropriate.

Morphometric quantification of trypsin and collagen. Digital images from immunohistochemistry and van Gieson staining were obtained using a Nikon E800 microscope with a ×10 objective lens (Nikon Instruments, Tokyo, Japan). Trypsin and collagen were quantified from 12 separate fields over 3 stained sections for each heart using Image Proplus software and expressed as percentages of the stained area per total myocardial tissue area.

Statistical analysis. Results are presented as means ± SD from 7–10 mice/group. Significance was calculated by one-way ANOVA. For survival analysis, the Gehan-Breslow-Wilcoxon test was used for the analysis of survival difference. P values of <0.05 were considered statistically significant.

RESULTS

Kinetics of body weight, survival rate, and myocardial inflammation as well as restoration by trypsin inhibitor. We have previously reported that the inflammatory response in the myocardium was most serious on *day 9* after viral infection (39). Biventricular dilation consistent with DCM was observed on *day 35* postinfection in male Balb/c mice and on *day 60* postinfection in male C3H/He mice (38, 46). Therefore, we observed the progression of myocardial inflammation from *day 9* to *60* postinfection. The severity of IAV infection was evaluated by weight loss, survival rate, and myocardial pathological changes. Mice intranasally inoculated with 40 plaque-forming units of IAV/PR/8 (H1N1) appeared lethargic and anorexic with significant weight loss in the acute stage ($P <$ 0.01; Fig. 1*A*). About 20–30% of mice died around *day 9* postinfection if not treated with aprotinin. No mice died after *day 20* postinfection (Fig. 1*B*). Surviving mice exhibited acute and chronic myocarditis, as confirmed by histological examination of hematoxylin and eosin-stained sections. Extensive inflammatory infiltration across the interstitium accompanied by focal necrosis and ECM destruction were observed on *day 9* in infected mice not treated with the trypsin inhibitor aprotinin. The prevalence of infiltration was alleviated by *day 20* postinfection but persisted with sparse, diffuse inflammatory cells in the interstitium on *day 60* postinfection (Fig. 1*C,1*). Aprotinin significantly reduced the loss of body weight, decreased morbidity, and suppressed the inflammatory response, which alleviated cardiac lesions (Fig. 1, *A*, *B*, and *C,2*).

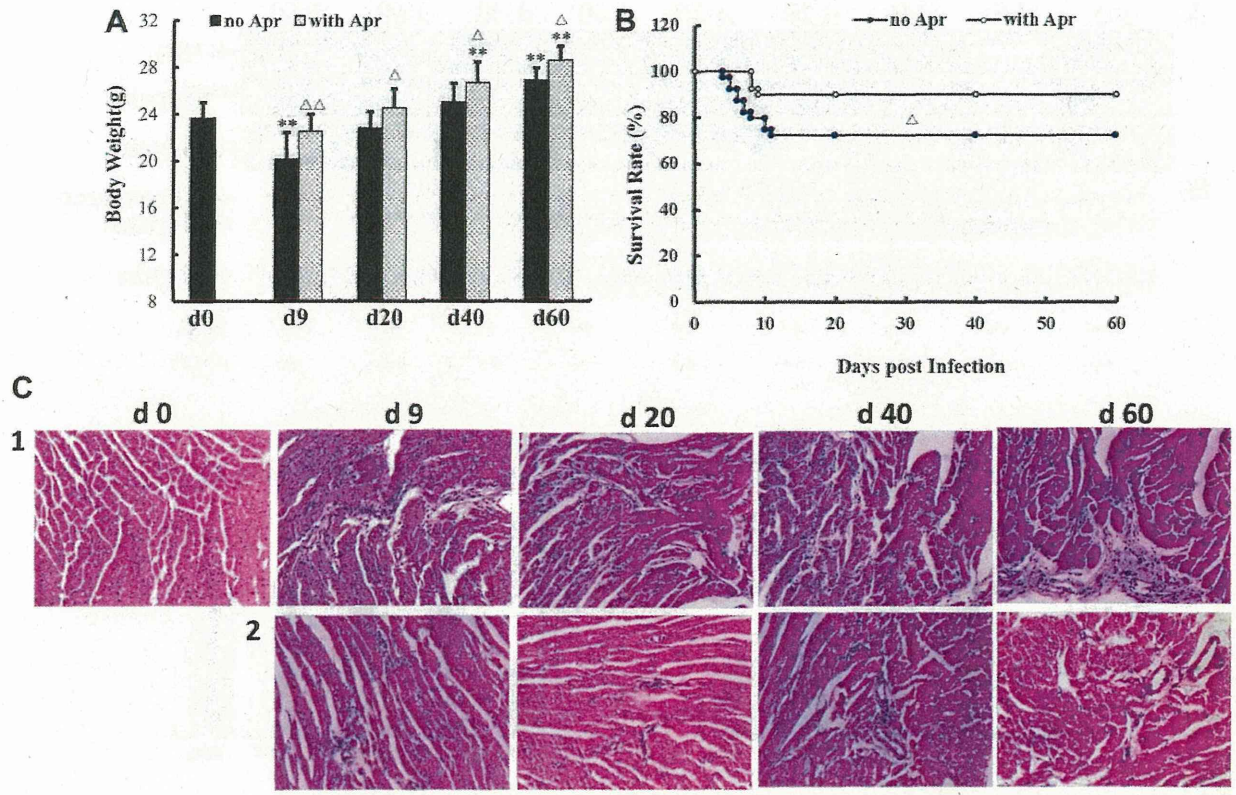

Fig. 1. Kinetics of body weight, survival rate, and myocardial inflammation. *A*: comparison of mouse body weights at different time points postinfection (n = 7–10 mice/group). $^{**}P < 0.01$ vs. *day* (d)*0*; $\triangle P < 0.05$ and $\triangle\triangle P < 0.01$ vs. no aprotinin (Apr) treatment at the same time point. *B*: Kaplan-Meier survival curve showing statistically significant differences in survival rates between mice treated with and without Apr (n = 40 mice with no Apr treatment and 40 mice with Apr treatment). $\triangle P < 0.05$ vs. no Apr treatment. *C*: myocardial inflammation monitored by hematoxylin and eosin staining from *days 0* to *60* postinfection without (*1*) and with (*2*) Apr treatment. Magnification: ×100.

Kinetics of viral replication and activation of trypsinogen with suppression by trypsin inhibitor. The kinetics of viral replication in hearts, as monitored by viral NS1 gene expression, showed that viral RNA peaked on *day 9* postinfection and then diminished to undetectable levels by *day 20* postinfection (Fig. 2*A*). Trypsin gene expression as monitored by RT-PCR and expression of trypsinogen plus trypsin and calculation of the trypsin-to-trypsinogen ratio based on Western blot analysis also peaked on *day 9* and then slowly declined to minimum levels by *day 60* postinfection, although levels were still higher than controls (*day 0*; Fig. 2, *A–D*). Immunofluorescent staining showed that trypsin distributed in the myocardium of infected loci during the acute stage. Immunohistochemical staining revealed that trypsin was mainly expressed by myocardial cells, which colocalized with inflammatory infiltrates (Fig. 2, *E* and *G*). The level of stained trypsin depositions quantified by area percentage was highest on *day 9* postinfection and declined gradually as myocardial inflammation declined during the chronic phase (*days 20* to *60* postinfection; Fig. 2*F*). Aprotinin significantly suppressed viral replication on *day 9* postinfection and inhibited upregulation of trypsin expression around inflammatory loci and the trypsin-to-trypsinogen ratio during both acute and chronic phases.

Kinetics of MMPs and cytokine upregulation by IAV and effects of trypsin inhibitor. The relationships among trypsin upregulation, MMP activation, and cytokine induction were analyzed in acute and chronic myocarditis. Along with an increase in trypsin levels, upregulated pro-MMP-9 was effectively converted to active MMP-9, although upregulated pro-MMP-2 was not activated (Fig. 3). MMP-9 activity, total MMP-9 (pro-MMP-9 plus active MMP-9) expression, and the active MMP-9-to-pro-MMP-9 ratio increased to a peak value on *day 9* postinfection followed by a slow decrease to *day 60* postinfection (Fig. 3). Similar induction time courses were observed for IL-6, IL-1β, and TNF-α (Fig. 4). Aprotinin significantly inhibited MMP-9 activity and suppressed upregulation of MMPs and activation of pro-MMP-9 as well as the induction of cytokines during acute and chronic myocarditis.

Increased Col I degradation in the myocardium was prevented by trypsin inhibitor. Both trypsin and MMP-9 efficiently degrade Col I (33, 37), and ICTP is released during hydrolysis of Col I fibrils. The amount of ICTP in the circulation is proportional to the amount of degraded fibrillar collagen (26). Therefore, ICTP was used as a marker for Col I degradation. Consistent with the observed changes in trypsin and MMP-9 expression, ICTP levels significantly increased on *day 9* postinfection and then slowly decreased from *day 20* postinfection, although on *day 60* postinfection levels did not match those in control mice. Aprotinin significantly decreased ICTP levels during acute and chronic phases, suggesting a prevention of Col I degradation (Fig. 5*A*).

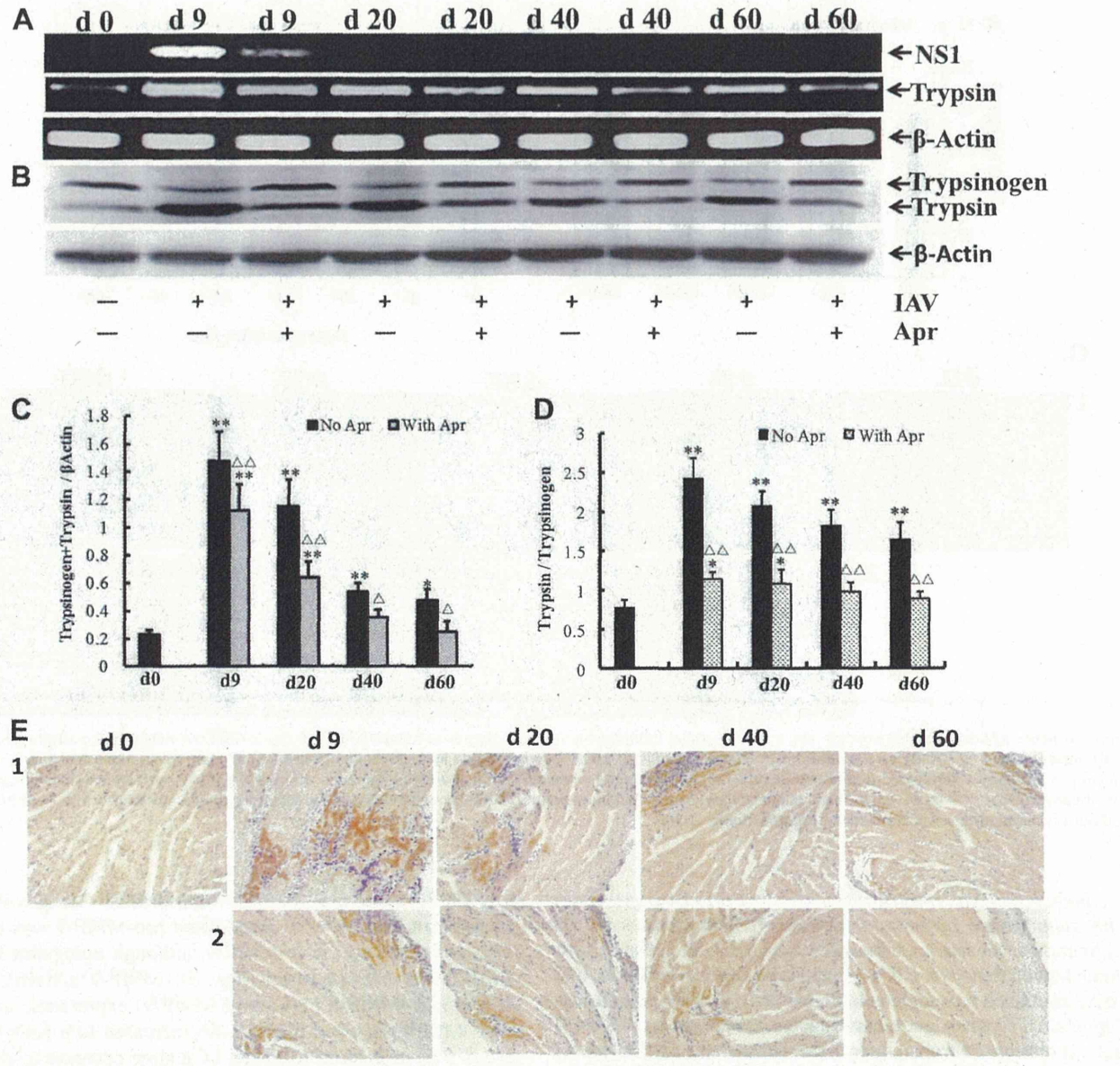

Fig. 2. Viral replication and activation of trypsinogen in the myocardium as well as colocalization of trypsin with inflammatory loci and influenza A virus (IAV). *A*: kinetics of viral nonstructural protein (NS)1 and trypsin gene expression by RT-PCR. *B*: expression of trypsinogen and trypsin by Western blot analysis. Band intensity was quantified by densitometry. β-Actin was the internal control. *C* and *D*: upregulation of trypsinogen + trypsin and activation of trypsinogen were significantly inhibited by Apr from *days 0* to *60* postinfection. Data are averages ± SD of 3 independent experiments from 7–10 mice/group. $^{*}P < 0.05$ and $^{**}P < 0.01$ vs. *day 0*; $\triangle P < 0.05$ and $\triangle\triangle P < 0.01$ vs. no Apr at the same observation time. *E*: immunohistochemical detection of upregulated trypsin in the myocardium without (*1*) and with (2) Apr treatment. *F*: quantified area percentage of trypsin ($n = 5$ mice/group). $^{**}P < 0.01$ vs. *day 0*; $\triangle\triangle P < 0.01$ vs. no Apr at the same observation time. *G*: representative immunofluorescent staining of IAV (green) and trypsin (red) in the myocardium without and with Apr treatment on *days 9* and *20* postinfection. Merged results are shown on the *right*. Magnification: ×100.

Increased collagen deposition in the myocardium reduced by trypsin inhibitor. During cardiac remodeling, loss of collagen from increased collagen degradation leads to replacement by newly synthesized collagen (21). To observe collagen proliferation and deposition after IAV infection, we used van Gieson staining. Heavy accumulation of collagen was seen around the blood vessels and inflammatory loci on *day 9* postinfection. From *day 20* postinfection, an extensive proliferation of collagen across the ventricular interstitium was observed and was most obvious on *day 60* postinfection. The increased collagen deposition was reduced in aprotinin-treated mice during acute and chronic phases (Fig. 5, *B* and *C*).

Increased Col I and Col III mRNA in the myocardium was suppressed by trypsin inhibitor. Cardiac ECM remodeling is associated with significant changes in Col I and Col III expression (45). Synthesis of Col I and Col III was assessed as Col I and Col III mRNA using RT-PCR. Both Col I and Col III mRNA significantly increased after IAV infection during acute and chronic phases (Fig. 5*D*). Myocardial Col I mRNA increased 2.9- to 1.8-fold from *days 9* to *60* postinfection (Fig.

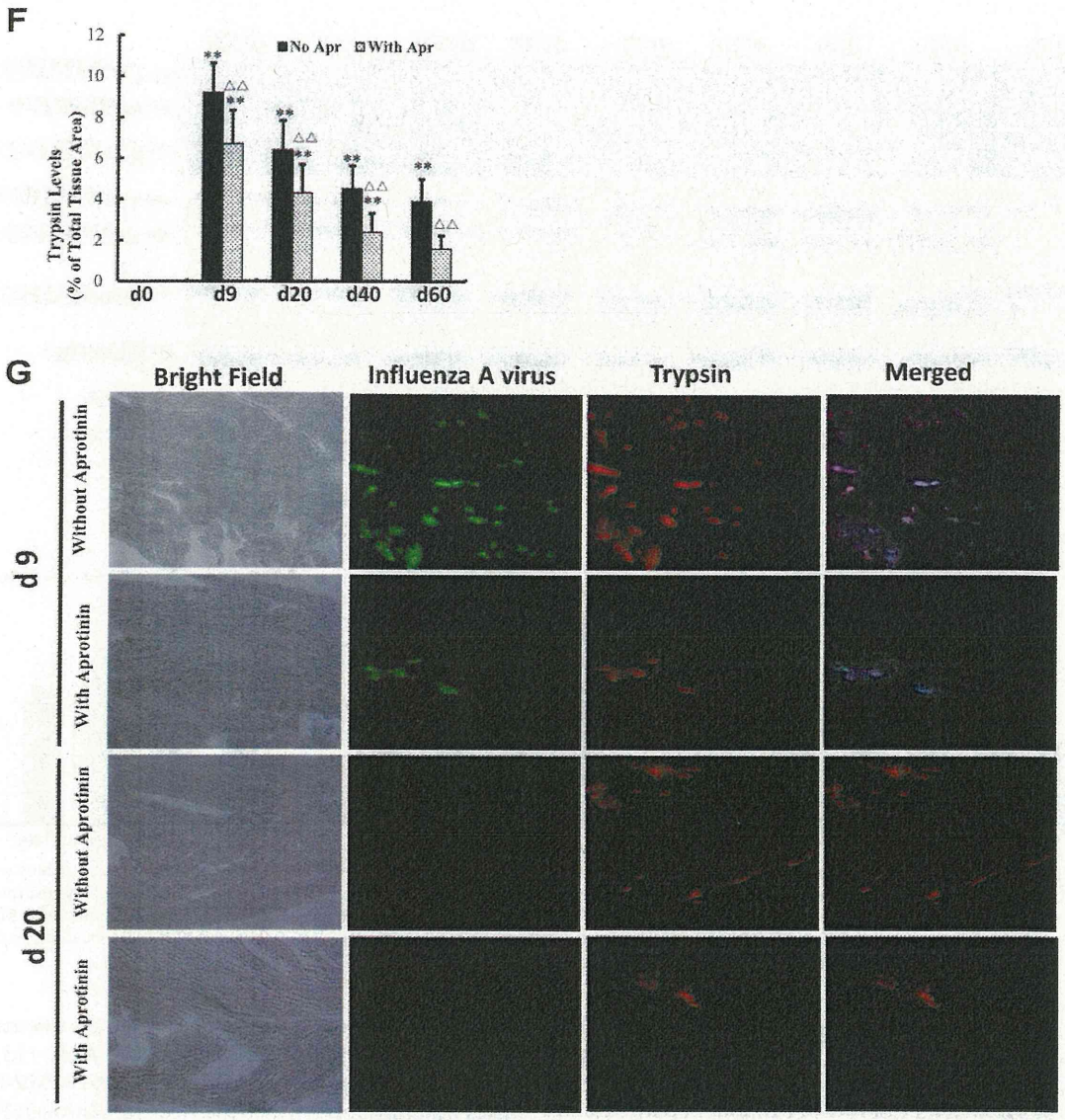

Fig. 2—*Continued*

5*E*). Col III mRNA increased 5.0- to 2.4-fold over the same time (Fig. 5*F*). The differential increase in Col I and Col III led to a decreased Col I-to-Col III ratio in IAV-induced acute and chronic myocarditis (Fig. 5*G*). Aprotinin significantly suppressed collagen upregulation and restored the Col I-to-Col III mRNA ratio.

LV dilation and cardiac dysfunction after IAV infection and effects of trypsin inhibitor. The dynamic changes of cardiac function, LV internal dimension, and LV posterior wall thickness were observed by echocardiography. IAV-infected mice were significantly impaired in LV function, as shown by a significant reduction in FS, EF, SV, and CO and a significant increase in LVESD on *day 9* postinfection, although LVEDD, LVPWd, and LVPWs values were similar to levels on *day 0*. LV function was transiently improved by alleviation of acute myocarditis on *day 20* postinfection and then deteriorated with progressive dilation of LV internal dimension and thinning of LV posterior wall thickness to *day 60* postinfection. Deterioration of cardiac function and dilation of heart chambers were improved significantly by aprotinin with increased values for FS, EF, SV, and CO, reduced values for LVEDD and LVESD, and restored values for LVPWd and LVPWs during acute and chronic myocarditis (Fig. 6 and Table 1).

DISCUSSION

We investigated the pathological mechanisms underlying the development of DCM from IAV-induced myocarditis. First, we found that IAV infection induced a persistent upregulation of ectopic trypsin, which localized in myocardial inflammatory loci, throughout acute and chronic stages. Persistently upregulated trypsin led to continuous activation of proMMP-9 and release of cytokines. Second, myocardial inflammatory infiltration persisted after IAV could not be detected in the myocardium. The severity of myocardial inflammation was consistent with the kinetics of trypsin expression. Third, Col I